Closing the gap: secular evolution of bar-induced dark gaps in the presence of thick discs

Soumavo Ghosh ,[1]★ Dimitri A. Gadotti ,[2] Francesca Fragkoudi ,[3] Vighnesh Nagpal,[4]
Paola Di Matteo[5] and Virginia Cuomo [6]

[1]*Max-Planck-Institut für Astronomie, Königstuhl 17, D-69117 Heidelberg, Germany*
[2]*Centre for Extragalactic Astronomy, Department of Physics, Durham University, South Road, Durham DH1 3LE, UK*
[3]*Institute for Computational Cosmology, Department of Physics, Durham University, South Road, Durham DH1 3LE, UK*
[4]*Department of Astronomy, University of California, Berkeley, CA 94720, USA*
[5]*GEPI, Observatoire de Paris, PSL Research University, CNRS, Place Jules Janssen, F-92195 Meudon, France*
[6]*Instituto de Astronomía y Ciencias Planetarias, Universidad de Atacama, Avenida Copayapu 485, 1530000 Copiapó, Atacama, Chile*

ABSTRACT

The presence of dark gaps, a preferential light deficit along the bar minor axis, is observationally well known. The properties of dark gaps are thought to be associated with the properties of bars, and their spatial locations are often associated with bar resonances. However, a systematic study, testing the robustness and universality of these assumptions, is still largely missing. Here, we investigate the formation and evolution of bar-induced dark gaps using a suite of N-body models of (kinematically cold) thin and (kinematically hot) thick discs with varying thick disc mass fractions and different thin-to-thick disc geometries. We find that dark gaps are a natural consequence of the trapping of disc stars by the bar. The properties of dark gaps (such as strength and extent) are well correlated with the properties of bars. For stronger dark gaps, the fractional mass-loss along the bar minor axis can reach up to ∼60–80 per cent of the initial mass contained, which is redistributed within the bar. These trends hold true irrespective of the mass fraction in the thick disc and the assumed disc geometry. In all our models harbouring slow bars, none of the resonances (corotation, inner Lindblad resonance, and 4:1 ultraharmonic resonance) associated with the bar correspond to the location of dark gaps, thereby suggesting that the location of dark gaps is not a *universal proxy* for these bar resonances, in contrast with earlier studies.

Key words: methods: numerical – galaxies: bar – galaxies: evolution – galaxies: kinematics and dynamics – galaxies: structure.

1 INTRODUCTION

A substantial fraction of disc galaxies in the local Universe harbour a stellar bar in the central region. The bar fraction reaches up to ∼50 per cent in optical wavelengths, while in infrared wavelengths, this bar fraction increases to around two-thirds of the whole disc galaxy population in the local Universe (e.g. see Eskridge et al. 2000; Menéndez-Delmestre et al. 2007; Nair & Abraham 2010; Masters et al. 2011; Buta et al. 2015; Kruk et al. 2017). Past observational studies revealed that the bar fraction and the bar properties vary with stellar mass and Hubble type (e.g. see Kormendy 1979; Aguerri et al. 2005; Marinova & Jogee 2007; Aguerri, Méndez-Abreu & Corsini 2009; Buta et al. 2010; Nair & Abraham 2010; Barway, Wadadekar & Kembhavi 2011; Gadotti 2011; Erwin 2018). High-redshift ($z \sim 1$) disc galaxies host prominent bars as well with the bar fraction decreasing with redshift (e.g. see Sheth et al. 2008; Melvin et al. 2014; Simmons et al. 2014, but also see Elmegreen, Elmegreen & Hirst 2004; Jogee et al. 2004). Recent *JWST* observations further revealed the presence of conspicuous bars even at higher redshifts ($z \sim 3$;

Costantin et al. 2023; Guo et al. 2023; Smail et al. 2023; Tsukui 2023; Le Conte et al. 2024). Several numerical studies demonstrated that in an N-body model, a bar often forms quite spontaneously (e.g. see Combes & Sanders 1981; Sellwood & Wilkinson 1993; Debattista & Sellwood 2000; Athanassoula 2003). Furthermore, cosmological simulations showed that bar formation already starts at $z \sim 1$ or more (e.g. see Kraljic, Bournaud & Martig 2012; Fragkoudi et al. 2020, 2021, 2024; Rosas-Guevara et al. 2022). At these redshifts, the discs are known to be kinematically hot (and turbulent) and more gas-rich, and possess a massive thick disc. However, recent N-body simulations (with both thin and thick discs) demonstrated that even in the presence of a massive thick disc (analogous to those high-redshift galaxies), bars and boxy/peanut bulges can form, purely from the internal gravitational instability (see Ghosh et al. 2023, 2024).

Past theoretical works demonstrated that as a bar grows over time, it continuously traps stars that are on nearly circular orbits on to the x_1 orbits that serve as a backbone for the bar structure (e.g. see Contopoulos & Grosbol 1989; Athanassoula 2003; Binney & Tremaine 2008). This transforms an initial azimuthally smooth light profile into a rather radially bright light profile, thereby causing a light deficit or 'dark gap' along the bar minor axis. The presence

★ E-mail: ghosh@mpia.de

of dark gaps has been shown observationally in barred galaxies (e.g. see Gadotti & de Souza 2003; Kim et al. 2016; Buta 2017). Using a sample of barred galaxies from the *Spitzer* Survey of Stellar Structure in Galaxies (S⁴G), Kim et al. (2016) showed that the strength of the dark gap is strongly related to the bar size and to bar-to-total light ratio, and the light deficit (along the bar minor axis) is directly proportional to bar size. In addition, Aguerri et al. (2023) showed that for about 90 per cent of their chosen sample of barred galaxies from the MaNGA (Mapping Nearby Galaxies at Apache Point Observatory) survey, the ratio of bar length to dark gap length remains greater than 1.2. Past *N*-body models showed that indeed the formation of dark gaps is linked with the growth of a stellar bar (e.g. see Kim et al. 2016; Ghosh & Di Matteo 2024) and dark gaps are more prominent and are located at larger radii as the bar evolves with time (Aguerri et al. 2023; Ghosh & Di Matteo 2024). Past studies have associated the location of the dark gap with different resonances of the bar. Buta (2017), using ∼50 early-to-intermediate-type barred galaxies, associated the location of the dark gaps with the corotation of the bar. On the other hand, recent studies by Krishnarao et al. (2022) and Aguerri et al. (2023), using a sample of MaNGA barred galaxies (and supplemented by an *N*-body model of a barred galaxy), showed that the locations of the dark gaps are associated with the 4:1 ultraharmonic resonance of the bar. However, a systematic study of the variation of properties of dark gaps with the properties of bars as well as testing the robustness and universality of the association of the location of dark gaps with different resonances (associated with the bar) is still missing. We aim to pursue this here.

In this work, we carry out a systematic study of the formation and temporal evolution of bar-driven dark gaps as well as the detailed study of the correlation (if any) between the properties of the dark gaps and the bar. To achieve that, we make use of a suite of *N*-body models with (kinematically hot) thick and (kinematically cold) thin discs, mimicking the presence of a thick disc in disc galaxies (e.g. see Pohlen et al. 2004; Yoachim & Dalcanton 2006; Comerón et al. 2016, 2019; Kasparova et al. 2016; Pinna et al. 2019a, b; Martig et al. 2021; Scott et al. 2021). Within the suite of *N*-body models, we vary the thick disc mass fraction as well as consider different geometric configurations (varying ratio of the thin and thick disc scale lengths). One of these models was studied in the context of properties of bars and boxy/peanut bulges (Fragkoudi et al. 2017) and the whole suite of models was studied concerning the formation of bars and boxy/peanut bulges in the presence of thick discs (Ghosh et al. 2023, 2024). Furthermore, as shown later in this work, the thin + thick models harbour a *slow bar*, i.e. with $R_{CR}/R_{bar} > 1.4$, where R_{CR} is the location of bar corotation and R_{bar} is the bar length (for further details, see Debattista & Sellwood 2000). Therefore, it is well suited to perform a systematic investigation of formation and evolution of bar-induced dark gaps as well as studying the correlation of their properties with bar properties. In addition, we present here a detailed investigation of the robustness and universality of the association of dark gaps with different bar resonances, which is largely missing in the literature.

The rest of the paper is organized as follows. Section 2 provides a brief description of the suite of *N*-body models used in this work. Section 3 presents our findings on the bar-induced dark gaps, their properties, and the temporal evolution as well as the correlation between the properties of the dark gaps and the bar. Section 4 presents the details of mass redistribution (within the bar region) as dark gaps grow over time. Section 5 contains the results of the robustness and universality of the association of dark gaps with different bar resonances. Section 6 summarizes the main findings of this work.

Table 1. Key structural parameters for the equilibrium models.

Model[a]	f_{thick} [b]	$R_{\text{d,thin}}$ [c] (kpc)	$R_{\text{d,thick}}$ [d] (kpc)
rthickS0.1	0.1	4.7	2.3
rthickE0.1	0.1	4.7	4.7
rthickG0.1	0.1	4.7	5.6
rthickS0.3	0.3	4.7	2.3
rthickE0.3	0.3	4.7	4.7
rthickG0.3	0.3	4.7	5.6
rthickS0.5	0.5	4.7	2.3
rthickE0.5	0.5	4.7	4.7
rthickG0.5	0.5	4.7	5.6
rthickS0.7	0.7	4.7	2.3
rthickE0.7	0.7	4.7	4.7
rthickG0.7	0.7	4.7	5.6
rthickS0.9	0.9	4.7	2.3
rthickE0.9	0.9	4.7	4.7
rthickG0.9	0.9	4.7	5.6

[a]Name of the model. [b]Thick disc mass fraction. [c]Scale length of the thin disc. [d]Scale length of the thick disc.

2 SIMULATION SET-UP AND *N*-BODY MODELS

To carry out a systematic study of the properties and the temporal evolution of dark gaps, we make use of a suite of *N*-body models, each consisting of a thin and a thick stellar disc, and the whole system is embedded in a live dark matter halo. One such model is already presented in Fragkoudi et al. (2017). In addition, these models have been thoroughly studied in recent works of Ghosh et al. (2023, 2024) in connection with bar and boxy/peanut formation scenarios under varying thick disc mass fractions. Here, we use a subsample (15 out of a total of 25 models) of the entire suite of thin + thick models to investigate bar-driven dark gaps and their temporal evolution with varying thick disc mass fractions.

The details of the initial equilibrium models are already provided in Fragkoudi et al. (2017) and Ghosh et al. (2023). For the sake of completeness, here we briefly mention the equilibrium models. Each of the thin and thick discs is modelled with a Miyamoto–Nagai profile (Miyamoto & Nagai 1975), having R_d, z_d, and M_d as the characteristic disc scale length, the scale height, and the total mass of the disc, respectively. The total stellar mass (thin and thick) is fixed to $1 \times 10^{11}\,\mathrm{M_\odot}$ for all the models considered here, while the fraction of stellar mass in the thick disc population (f_{thick}) varies from 0.1 to 0.9. The scale heights of the thin and thick discs are fixed at 0.3 and 0.9 kpc, respectively. The dark matter halo is modelled by a Plummer sphere (Plummer 1911), having $R_H (= 10\,\mathrm{kpc})$ and M_{dm} $(= 1.6 \times 10^{11}\,\mathrm{M_\odot})$ as the characteristic scale length and the total halo mass, respectively. The dark matter halo parameters are kept fixed across the suite of thin + thick models considered here. The values of the key structural parameters for the thin and thick discs are mentioned in Table 1. For this work, we analysed a total of 15 *N*-body models of such thin + thick discs.

A total of 1×10^6 particles are used to model the stellar (thin + thick) disc, while a total of 5×10^5 particles are used to model the dark matter halo. The initial conditions of the discs are obtained using the iterative method algorithm (for details, see Rodionov, Athanassoula & Sotnikova 2009). For this work, we only constrained the density profile of the stellar discs, while allowing the velocity dispersions (specifically the radial and vertical components) to vary in such a way that the system converged to an equilibrium solution. The corresponding radial profiles of velocity dispersion are shown in Fragkoudi et al. (2017, see their fig. 1). For further
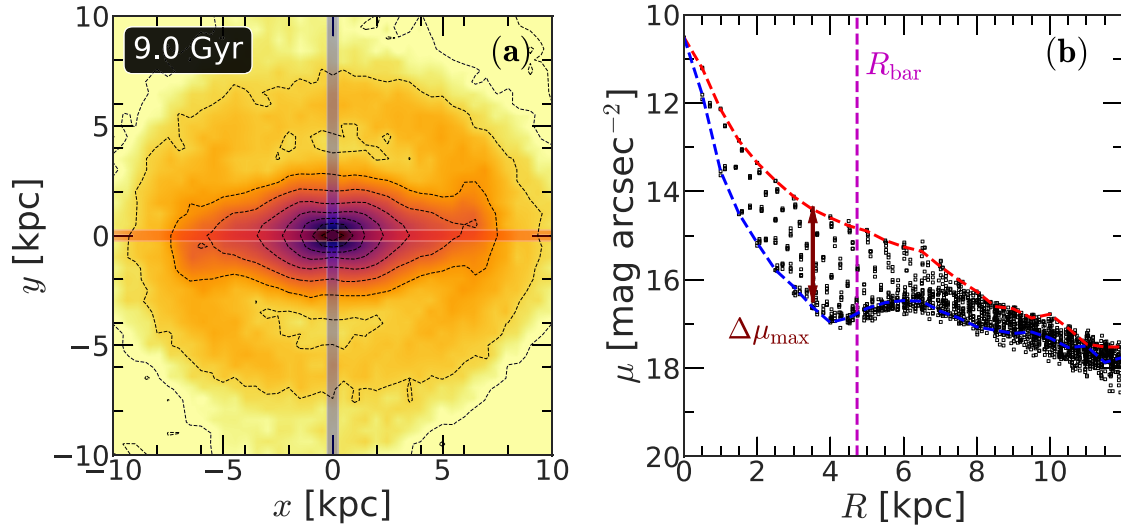
Figure 1. Left panel: Face-on surface brightness distribution, calculated using $\Upsilon_T/\Upsilon_t = 1.2$ (mass-to-light ratio for thick and thin disc stars) at $t = 9\,\mathrm{Gyr}$ for the model rthickS0.1. The dashed black lines denote the contours of constant surface brightness. Here, a conversion of 1 arcsec = 1 kpc and a magnitude zero-point (m_0) of 22.5 mag arcsec^{-2} are used to create the surface brightness map from the intrinsic particle distribution. The red and blue lines denote the bar major and minor axes, respectively. Right panel: Corresponding light profiles along the bar major and minor axis (red and blue dashed lines, respectively). The radial location where the light deficit around the bar reaches its maximum ($\Delta\mu_{\max}$) is indicated by the maroon arrow. The vertical magenta line denotes the bar length, R_{bar}. Each solid square represents a single pixel of the face-on surface brightness map.

details, the reader is referred to Fragkoudi et al. (2017) and Ghosh et al. (2023). The simulations are run using a TREESPH code by Semelin & Combes (2002). A hierarchical tree method (Barnes & Hut 1986) with an opening angle $\theta = 0.7$ is used for calculating the gravitational force that includes terms up to the quadrupole order in the multipole expansion. A Plummer potential is employed for softening the gravitational forces with a softening length $\epsilon = 150\,\mathrm{pc}$. We evolved all the models for a total time of 9 Gyr.

Within the suite of thin + thick disc models, we considered three different scenarios for the scale lengths of the two disc (thin and thick) components. In rthickE models, $R_{\mathrm{d,thick}} = R_{\mathrm{d,thin}}$; in rthickS models, $R_{\mathrm{d,thick}} < R_{\mathrm{d,thin}}$; and in rthickG models, $R_{\mathrm{d,thick}} > R_{\mathrm{d,thin}}$, where $R_{\mathrm{d,thin}}$ and $R_{\mathrm{d,thick}}$ denote the scale length for the thin and thick disc, respectively. Following Ghosh et al. (2023), any thin + thick model is referred to as a unique string '[MODEL CONFIGURATION][THICK DISC FRACTION]'. [MODEL CONFIGURATION] denotes the corresponding thin-to-thick disc scale length configuration, i.e. rthickG, rthickE, or rthickS, whereas [THICK DISC FRACTION] denotes the fraction of the total disc stars that are in the thick disc population (or equivalently, the mass fraction in the thick disc as all the disc particles have same mass).

3 PROPERTIES OF DARK GAPS AND THEIR CORRELATION WITH BAR PROPERTIES

Fig. 1 (left panel) shows the face-on surface brightness distribution (in mag arcsec^{-2}) for the model rthickS0.1, calculated at the end of the simulation run ($t = 9\,\mathrm{Gyr}$). We used a magnitude zero-point (m_0) of 22.5 mag arcsec^{-2} to create the surface brightness map from the intrinsic particle distribution. The same magnitude zero-point is used throughout this work. In addition, a conversion of 1 kpc = 1 arcsec is used throughout this work. This would place the mock galaxies (produced from the thin + thick models) at a redshift $z \sim 0.05$ with an assumed ΛCDM (Lambda cold dark matter) cosmology with parameters $\Omega_m = 0.315$ and $H_0 = 67.4\,\mathrm{km\,s^{-1}\,Mpc^{-1}}$ (Planck

Collaboration VI 2020). Moreover, we assumed a mass-to-light ratio (Υ) in order to convert the mass distribution to the light distribution. Since our models include both the thin and thick disc stars, therefore, a reasonable choice for the Υ_T/Υ_t is required, where Υ_T and Υ_t denote the assumed mass-to-light ratio for the thick and thin disc stars, respectively. Following Comerón et al. (2011), we assumed three values of Υ_T/Υ_t in this work, namely $\Upsilon_T/\Upsilon_t = 1$, 1.2, and 2.4 (for details see Comerón et al. 2011), and further checked how these assumed values of Υ_T/Υ_t affect the results concerning the strength and extent of dark gaps. Even a mere visual inspection of Fig. 1 reveals the presence of a conspicuous dark gap, along the bar minor axis, for the model rthickS0.1. In Appendix A, we show the face-on surface brightness distribution (in mag arcsec^{-2}), calculated at $t = 9\,\mathrm{Gyr}$, for all thin + thick models considered here (see Fig. A1). The presence of prominent dark gaps, for almost all the thin + thick models, is evident from Fig. A1, similarly to the model rthickS0.1 shown here. In what follows, we quantify the strength and the extent of the dark gaps and then investigate their temporal evolution with varying f_{thick} values.

To this aim, we first extract the surface brightness profiles along the bar major and minor axis while putting a slit of width, $\Delta = 0.5\,\mathrm{kpc}$, in each direction. Following Kim et al. (2016), at time t, we define the strength of the dark gap as the maximum light deficit, $\Delta\mu_{\max}$, between the bar major and minor axis. By definition, it is a non-negative quantity. In addition, we define the extent of the dark gap, R_{DG}, where the maximum light deficit ($\Delta\mu_{\max}$) occurs, i.e. $\Delta\mu(R = R_{\mathrm{DG}}) = \Delta\mu_{\max}$. An example of determining the $\Delta\mu_{\max}$ and R_{DG} is also shown in Fig. 1 (right panel) for the model rthickS0.1.

First, we investigate how the strength of the dark gaps is related to the bar strength. The bar strength, S_{bar}, at time t is defined as the maximum of the $m = 2$ Fourier coefficient (A_2/A_0), i.e. $S_{\mathrm{bar}}(t) = \max\{(A_2/A_0)(R, t)\}$, and these values are taken from Ghosh et al. (2023). The resulting correlation between the strengths of the dark gap and the bar, for the three assumed values of Υ_T/Υ_t, namely $\Upsilon_T/\Upsilon_t = 1$, 1.2, and 2.4, for all thin + thick models considered here,

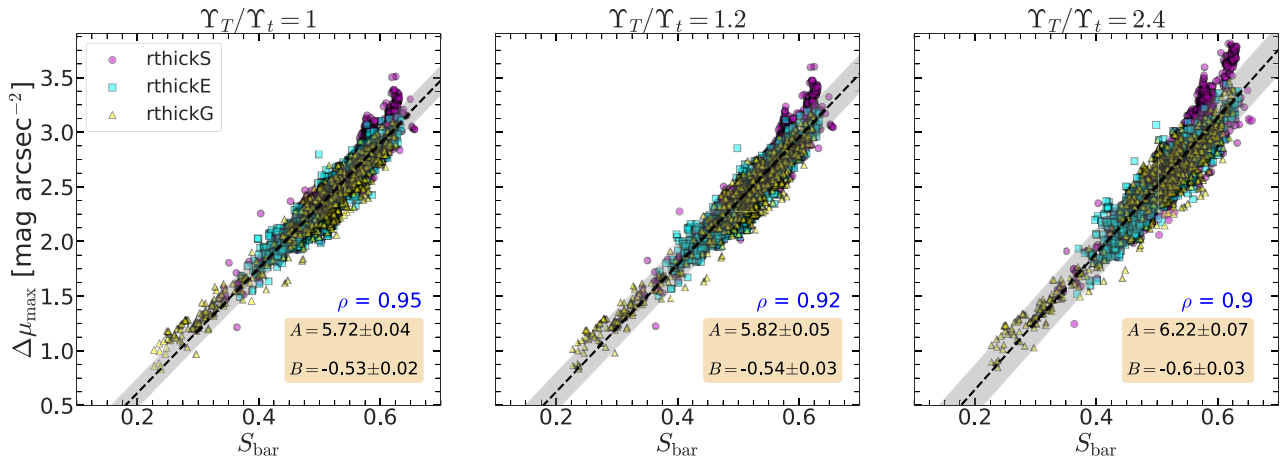**Figure 2.** Correlation between the bar strength, S_{bar}, and the strength of the dark gap, $\Delta\mu_{max}$, for all 15 thin + thick models considered here. Left panel shows the correlation for $\Upsilon_T/\Upsilon_t = 1$, while the middle panel and right panel show the corresponding correlation for $\Upsilon_T/\Upsilon_t = 1.2$ and 2.4, respectively. The magenta circles denote the snapshots from the rthickS models, whereas the cyan squares and the yellow triangles denote the snapshots from the rthickE and rthickG models, respectively. The black dash line denotes the best-fitting straight line (of the form $Y = AX + B$), while the grey shaded region denotes the 3σ scatter around the best-fitting line. These two quantities remain strongly correlated (Pearson correlation coefficient $\rho > 0.75$) throughout the entire temporal evolution.

are shown in Fig. 2. Note that in Fig. 2 only the snapshots after the bar forms are considered for all thin + thick models. Following Ghosh et al. (2024), we define the bar formation epoch τ_{bar} as the epoch when the amplitude of the $m = 2$ Fourier moment becomes greater than 0.2 and the corresponding phase angle ϕ_2 remains constant (within $3°$–$5°$) within the extent of the bar. Therefore, the bar age is defined as $t_{bar\,age} = t - \tau_{bar}$. Furthermore, we computed the Pearson correlation coefficient ρ to quantify the correlation. As seen clearly, when all the thin + thick models are taken together, the bar strength and the strength of the dark gaps remain strongly correlated ($\rho > 0.75$) for all three assumed values of Υ_T/Υ_t. This is not surprising since the bar strength is defined as a maximum of the $m = 2$ Fourier coefficient of the density at a radial location R, and the dark gap strength is the (light-weighted and smoothed) peak-to-trough ratio of the density. Therefore, in the limit where the density variation is sinusoidal with respect to the azimuthal angle and the mass-to-light ratio is constant, these are perfectly correlated by construction. Fig. 2 essentially demonstrates the fact that altering the mass-to-light ratio of the two components (thin and thick disc) does not significantly affect the fundamental conclusion that the strengths of bar and dark gap are inherently correlated.

Next, we investigate how the extent of the dark gaps, R_{DG}, evolves with time, and if there exists any correlation between the extent of the dark gap and the length of the bar, in our thin + thick models. Following Ghosh & Di Matteo (2024), we define the bar length, R_{bar}, as the radial extent where the amplitude of the $m = 2$ Fourier moment (A_2/A_0) drops to 70 per cent of its peak value. We checked that the ratio R_{bar}/R_{DG} always remains well above 1.2, at all times, for all thin + thick models. For the sake of brevity, they are not shown here. This finding is in agreement with Aguerri et al. (2023) who showed that for a majority (about 90 per cent) of their sample of barred galaxies from the MaNGA survey, the ratio R_{bar}/R_{DG} remains above 1.2.

Lastly, we investigate if there exists any correlation between the bar length and the extent of the dark gap. This is shown in Fig. 3 for all thin + thick models considered here. As seen from Fig. 3, the Pearson correlation coefficient ρ remains well above 0.75 for almost all models, thereby indicating that the bar length and extent of the

dark gap are strongly correlated. However, for the models rthickS0.9 and rthickG0.9, the bar length and extent of the dark gap are not correlated (see the corresponding ρ values in Fig. 3). We recall that R_{DG} is defined as the location where the maximum of peak-to-trough variation (along bar major and minor axes) occurs, whereas R_{bar} is defined where the A_2/A_0 value drops to 70 per cent of its peak value. Therefore, the question remains whether the temporal evolution of R_{DG} in these two models signifies a different evolutionary scenario for the dark gaps or is it due to the different definitions of R_{DG} and R_{bar} (one locating the peak while the other extends beyond the peak location). To verify that, we first calculated the radial profiles of $\Delta\mu$ for the three thin + thick models, namely rthickS0.1, rthickS0.7, and rthickS0.9. This is shown in Appendix A (see Fig. A2 there). As seen clearly from Fig. A2, the peak location of $\Delta\mu$ moves progressively towards the outer disc as the bar (and the dark gaps grow in strength) for the model rthickS0.1. However, for the model rthickS0.9, the peak location of $\Delta\mu$ does not move as much towards the outer disc region over time. This explains why R_{DG} values remain almost constant for the model rthickS0.9. The trend for the model rthickS0.7 falls somewhere in between these two above-mentioned trends. Lastly, to check whether a difference in defining R_{DG} and R_{bar} (one locating the peak while the other extends beyond the peak location) impacts the inference of correlation between the length of bars and dark gaps, we introduce a new metric to define the extent of the dark gap, namely R_{dark} that is defined as the location where $\Delta\mu$ value falls to 70 per cent of its peak value. The corresponding correlation between R_{bar} and R_{dark}, computed for the models rthickS0.9 and rthickG0.9, is shown in Fig. 4. As seen clearly from Fig. 4, R_{bar} and R_{dark} remain strongly correlated ($\rho > 0.75$) for the models rthickS0.9 and rthickG0.9. We checked that R_{bar} and R_{dark} remain strongly correlated for other thin + thick models as well. For the sake of brevity, we have not shown it here. This emphasizes that when a uniform definition is used to define the bar length and the length of the dark gap, they remain strongly correlated over the entire evolutionary phase. A similar discrepancy exists in measuring the bar length from the peak location of the A_2/A_0 value and the location where the A_2/A_0 value drops to the 70 per cent of its peak value (for further details, see Ghosh & Di Matteo 2024). Our findings here outline the importance of a uniform
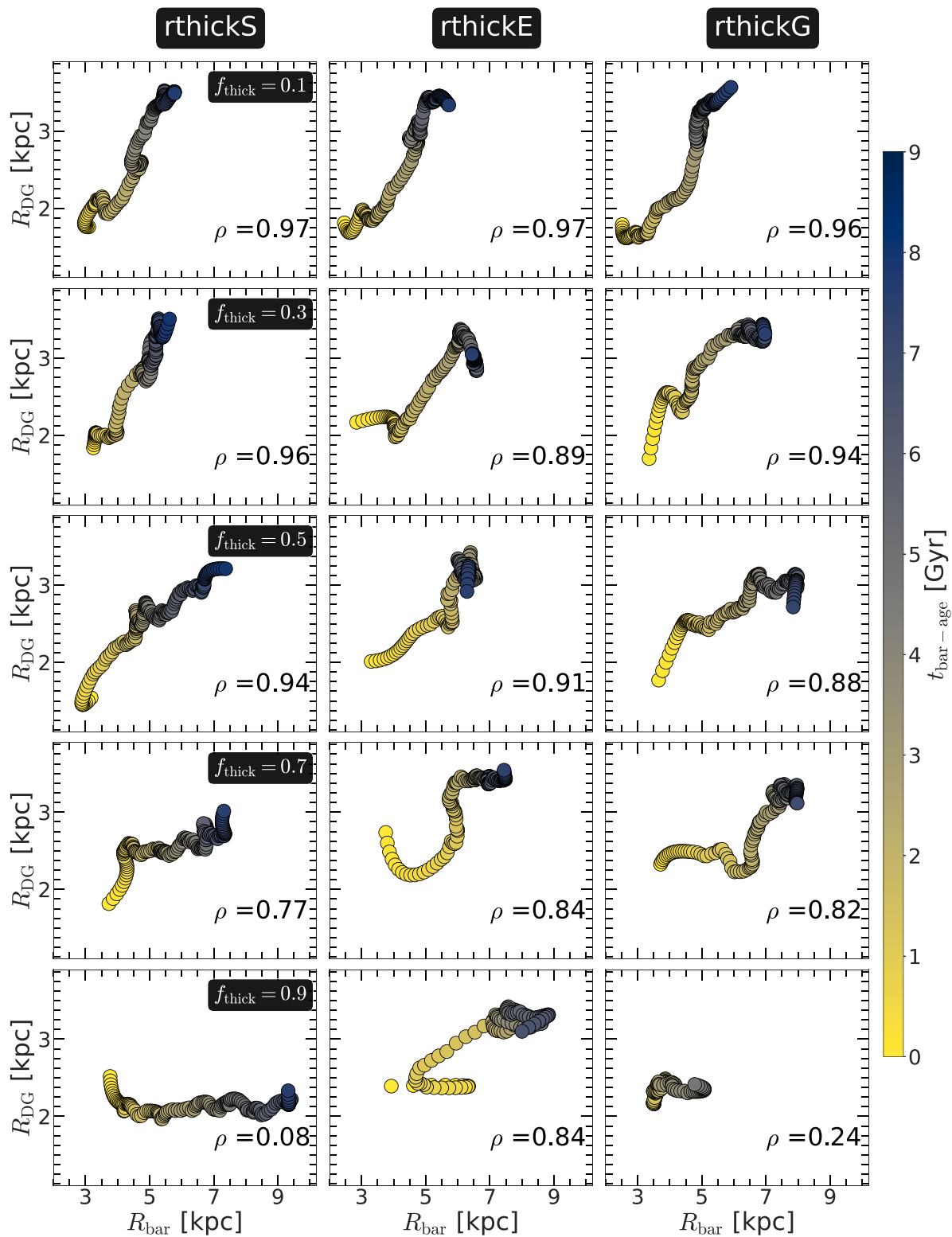
Figure 3. Correlation between the bar length, R_{bar}, and the extent of the dark gap, R_{DG}, calculated for all thin + thick models, as a function of the bar age (see the colour bar). Left panels correspond to the rthickS models, whereas middle panels and right panels correspond to the rthickE and rthickG models, respectively. The thick disc fraction (f_{thick}) varies from 0.1 to 0.9 (top to bottom), as indicated in the leftmost panel of each row. In each case, the Pearson correlation coefficient ρ is calculated, and the corresponding value is quoted in each panel. These two quantities remain strongly correlated (Pearson correlation coefficient $\rho > 0.75$) for all the thin + thick models, except for the models rthickS0.9 and rthickG0.9. For further details, see the text.
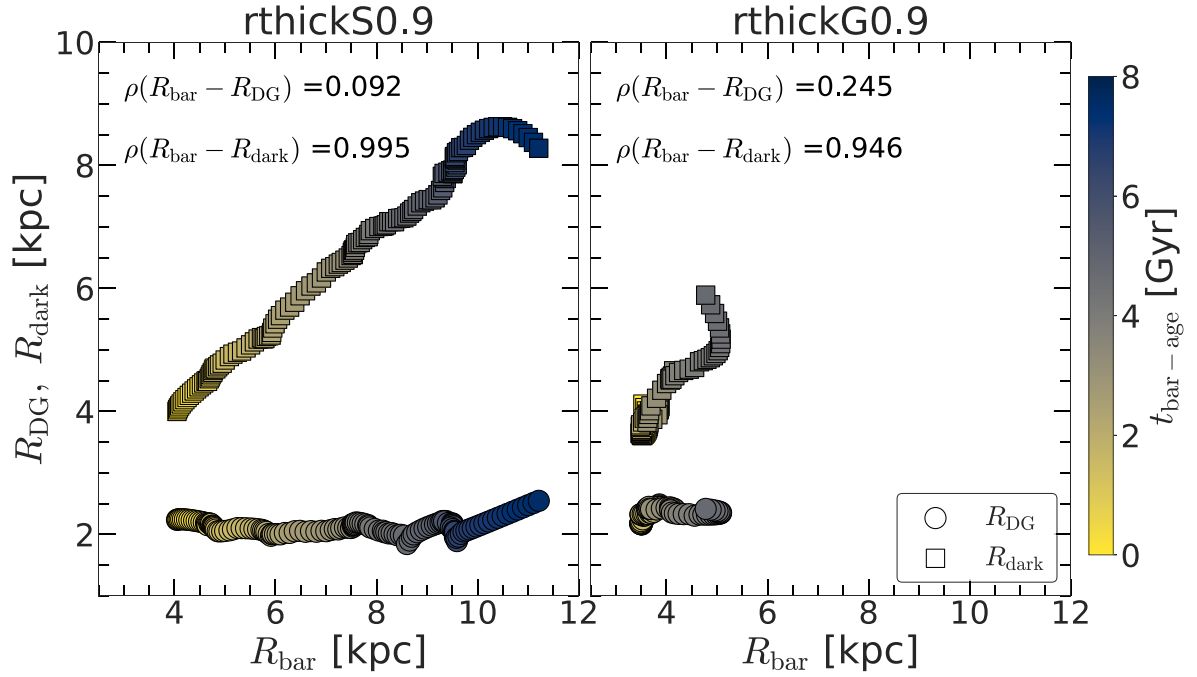
Figure 4. Correlation between the bar length, R_{bar}, and the extent of the dark gap, R_{DG} (in open circles), and between R_{bar} and R_{dark} (in open squares), calculated for the two thin + thick models, namely rthickS0.9 (left panel) and rthickG0.9 (right panel), as a function of the bar age (see the colour bar). In each case, the Pearson correlation coefficient ρ is calculated, and the corresponding values are quoted. The two quantities R_{bar} and R_{dark} remain strongly correlated (Pearson correlation coefficient $\rho > 0.75$) for the models rthickS0.9 and rthickG0.9.

definition for the bar and dark gap lengths, and demonstrate how different definitions for the bar and dark gap lengths might lead to an erroneous conclusion.

To conclude, our systematic study demonstrates that the dark gap in a disc galaxy is essentially a part and parcel of the dynamical effect of a bar as the bar continuously redistributes the stars on to more radially elongated orbits, thereby producing a dearth of stellar density along the bar minor axis. The strength and the extent of these dark gaps can be used a robust proxy for the bar strength and length, respectively. This has a direct implication for the observational study of the dark gap and the bar properties. For a barred galaxy, observed at an intermediate inclination, the quantification of bar strength (calculated via the $m = 2$ Fourier coefficient) can often be cumbersome, involving deprojection of the image (and associated uncertainty) and also critically depends on the resolution of the photometric image. As our findings demonstrate, the strength of the dark gaps, which are quite straightforward to compute for an observed galaxy, can serve as an excellent proxy for the bar strength. A similar argument applies to using the extent of the dark gaps as an excellent proxy for the bar length as well.

4 GROWTH OF DARK GAPS AND THE ASSOCIATED MASS REDISTRIBUTION

In the previous section, we demonstrated that the properties (strength and extent) of the dark gaps show a strongly correlated evolution with the bar properties (strength and length) in all thin + thick models considered here. As the bar grows in strength, it continuously traps more stars into more radially elongated orbits, thereby making an initial azimuthally uniform light profile into a rather radially bright light profile. Since we are dealing with N-body models here, and therefore, without any assumption of mass-to-light (M/L) ratio (as

commonly done in observations), we can quantify the mass-loss along the bar minor axis as the dark gaps grow with time. To quantify the fractional mass change in the ($x-y$) plane (face-on configuration) at time t, we define

$$\delta M_*(x, y, t) = \frac{M_*(x, y, t) - M_*(x, y, t = 0)}{M_*(x, y, t = 0)}, \quad (1)$$

where $M_*(x, y, t)$ denotes the stellar (thin + thick) mass at the spatial location (x, y) at time t. The corresponding face-on distribution of the fractional mass change at different times (capturing different phases of bar evolution) is shown in Fig. 5 for the model rthickS0.1. As seen clearly from Fig. 5, stellar mass gets enhanced along the bar major axis, and simultaneously there is a continuous mass deficit along the bar minor axis. At times, when the bar (and hence, the dark gaps) is quite strong, the mass deficit along the bar minor axis can reach up to $\sim$60–80 per cent of its initial ($t = 0$) mass.

Next, to quantify the fractional mass change, at time t, along the bar minor axis, we define

$$\delta M_*(y_{minor}, t) = \frac{M_*(y_{minor}, t) - M_*(y_{minor}, t = 0)}{M_*(y_{minor}, t = 0)}, \quad (2)$$

where y_{minor} denotes the spatial location along the bar minor axis, and $M_*(y_{minor}, t)$ denotes the stellar mass at a spatial location y_{minor} along the bar minor axis at time t. A positive value of $\delta M_*(y_{minor}, t)$ denotes mass increase, whereas a negative value of $\delta M_*(y_{minor}, t)$ denotes mass-loss at a certain time t. The corresponding temporal evolution of $\delta M_*(y_{minor}, t)$, calculated with $\Delta y_{minor} = 1$ kpc, for the thin + thick model rthickS0.1 is shown in Fig. 6. As seen from Fig. 6, spatial location corresponding to $y_{minor} < 1$ kpc falls in the part of the bar structure, and it shows substantial mass increase (compare Figs 5 and 6). However, spatial locations falling within the region of dark gap ($1 < y_{minor}/kpc < 5$) show substantial mass-loss (i.e.
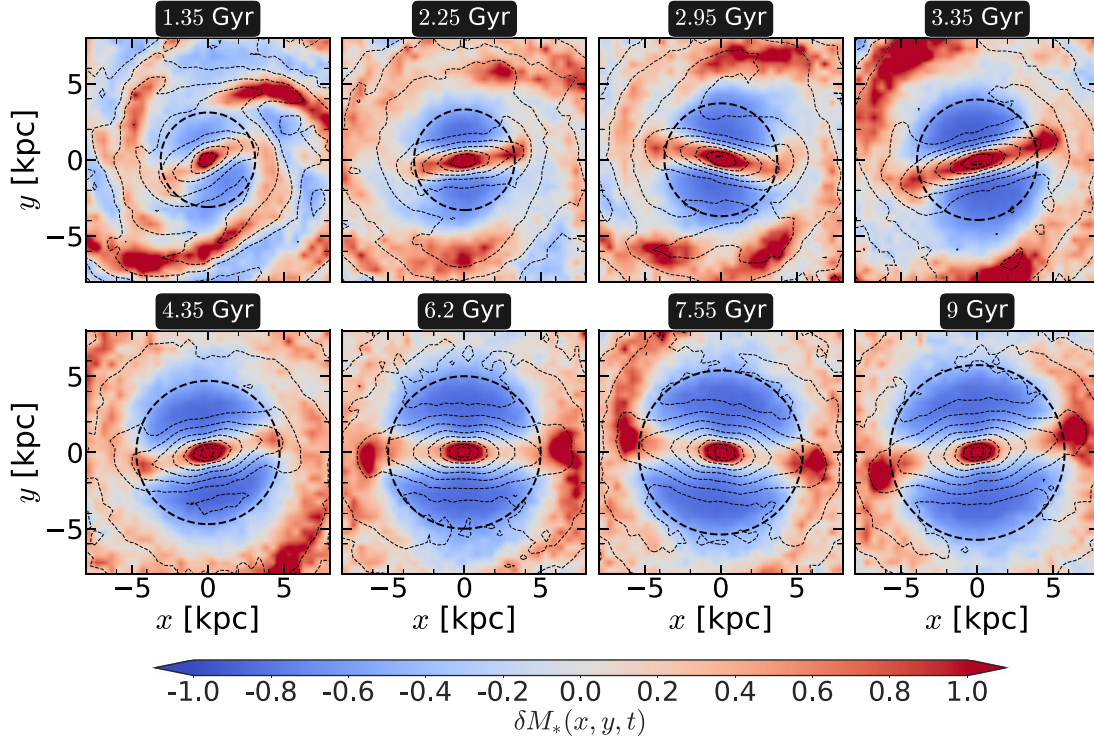
Figure 5. Face-on distribution of the fractional mass change, $\delta M_*(x, y, t)$ (see equation 1), at different times (capturing different phases of bar evolution) for the model rthickS0.1. A positive $\delta M_*(x, y, t)$ denotes the mass gain, while a negative $\delta M_*(x, y, t)$ implies mass-loss at a location (x, y). The black dashed lines denote the contours constant surface density. The black circle denotes the bar length, R_{bar}. As the bar evolves with time, stellar mass gets enhanced along the bar major axis (see the red regions), and simultaneously there is a continuous mass deficit along the bar minor axis (see the blue regions).
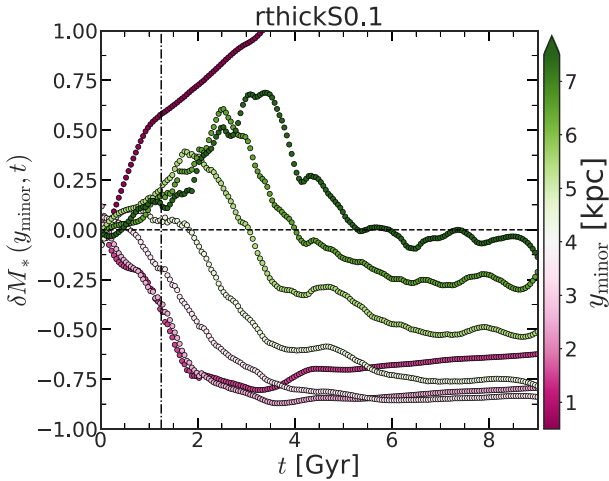
Figure 6. Fractional mass-loss, at different spatial locations along the bar minor axis, $\delta M_*(y_{minor}, t)$ (equation 2), as a function of time for the thin + thick model rthickS0.1. The colour bar shows the spatial locations along the bar minor axis. The vertical dash–dotted line denotes the epoch of bar formation τ_{bar}. $1 < y_{minor}/\text{kpc} < 5$ denotes the region of the dark gap. For details, see Section 4.

$\delta M_*(y_{minor}, t) < 0$) over the course of the evolution. The temporal evolution of $\delta M_*(y_{minor}, t)$ beyond $y_{minor} = 6$ kpc shows a moderate increase at initial times, and this is due to the fact that over time the disc grows in the outward direction.

Lastly, to carry out a uniform comparison of fractional mass-loss (within the extent of the bar) along the bar minor axis for all the thin + thick models considered here, we define

$$\Delta M_{*, minor}(t_{end})$$
$$= \frac{\int_{R_{in}}^{R_{bar}} \left[M_{*, minor}(R, t_{end}) - M_{*, minor}(R, t = 0) \right] \mathrm{d}R}{\int_{R_{in}}^{R_{bar}} M_{*, minor}(R, t = 0) \, \mathrm{d}R}, \qquad (3)$$

where we assumed $R_{in} = 0.5$ kpc and $M_{*, minor}(R, t)$ is the mass at a radial location R at time t along the bar minor axis. In Fig. 7 (left panel), we show one such example of the fractional mass-loss along the bar minor axis for the model rthickS0.1 (see the grey shaded region). Next, we compute the fractional mass-loss (within the extent of the bar) along the bar minor axis using equation (3) for all the thin + thick models considered here. This is shown in Fig. 7 (right panel). The fractional mass-loss (within the extent of the bar) along the bar minor axis, calculated at the end of the simulation run ($t_{end} = 9$ Gyr), is strongly correlated with the maximum light deficit $\Delta\mu_{max}$. For some thin + thick models showing stronger dark gaps (and harbouring stronger bar), the fractional mass-loss (within the extent of the bar) along the bar minor axis can reach up to ~80 per cent of the initial mass contained within the bar region (see right panel of Fig. 7). This strong correlation between the $\Delta M_{*, minor}(t_{end})$ and $\Delta\mu_{max}(t_{end})$ further supports the scenario of the growth of dark gaps as a result of continuous trapping of stars that are on nearly circular orbits on to the more elongated orbits by the bar.
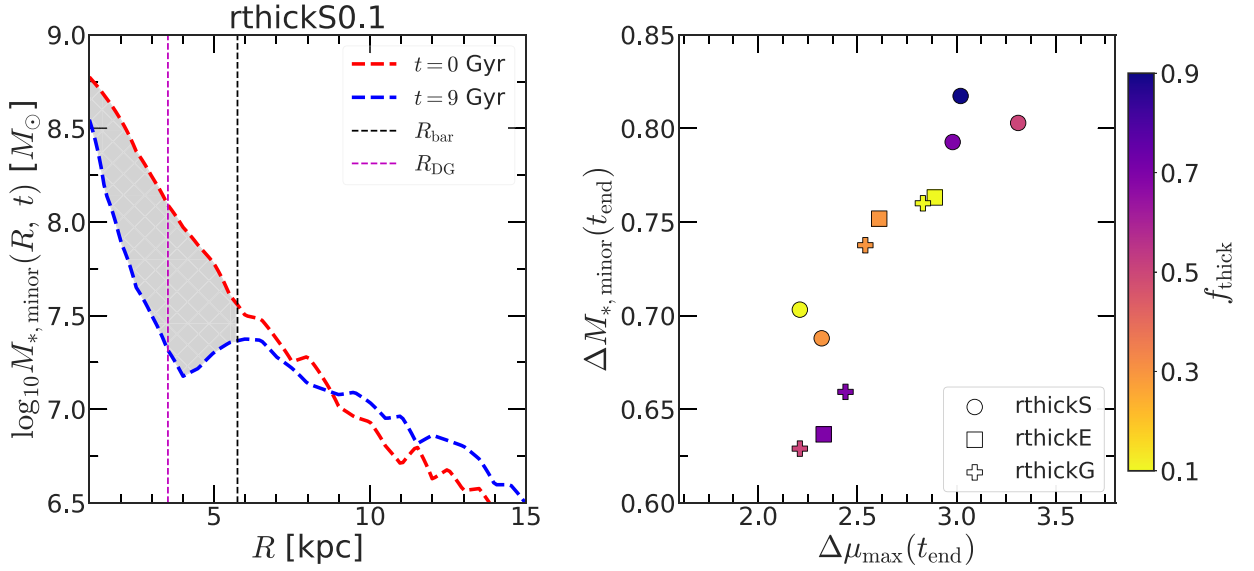
Figure 7. Left panel: Radial distribution of stellar (thin + thick) mass (in logarithmic scale), along the bar minor axis, at the beginning and at the end of the simulation run ($t_{end} = 9\,\mathrm{Gyr}$), for the model rthickS0.1. The vertical black dashed line denotes the bar extent (R_{bar}), while the vertical magenta dashed line denotes the extent of the dark gap (R_{DG}) at $t = t_{end}$. The grey shaded region denotes the fractional mass-loss, $\Delta M_{*,minor}(t_{end})$ (see equation 3), along the bar minor axis. Right panel: Correlation between the fractional mass-loss along the bar minor axis ($\Delta M_{*,minor}(t_{end})$) and the strength of the dark gap $\Delta \mu_{max}(t_{end})$ for all thin + thick models considered here. The thick disc mass fraction (f_{thick}) is shown in the colour bar. $\Upsilon_T / \Upsilon_t = 1.2$ is used to compute the values of $\Delta \mu_{max}$.

5 DARK GAPS AND RESONANCE LOCATIONS

Past studies have associated the location of the dark gap (R_{DG}) with different resonances of the bar (for details, see Section 1 and references therein). However, the robustness and universality of this trend have not been tested so far in the literature. We pursue it here.

In order to measure the correlation between the extent of the dark gaps and different resonances (associated with the bar), first we need to compute the circular velocity (v_c) and the bar pattern speed (Ω_{bar}) at different times for all thin + thick models considered here. At time t, the circular velocity v_c is calculated as

$$v_c^2(R) = \frac{GM(\leq r)}{r}. \tag{4}$$

Here, $M(\leq r)$ denotes the mass enclosed within a spherical radius r. Once we derive the circular velocity, the corresponding circular frequency Ω and the epicyclic frequency κ are derived using $\Omega = v_c/R$ and $\kappa^2 = 4\Omega^2 + d\Omega^2/dR$ (for details, see Binney & Tremaine 2008). The corresponding radial profiles of Ω, κ, $\Omega - \kappa/2$, and $\Omega - \kappa/4$ calculated at $t = 1.35\,\mathrm{Gyr}$ for the model rthickS0.1 are shown in Fig. 8.

In order to determine the location for the corotation, the 2:1 inner Lindblad resonance, and the 4:1 ultraharmonic resonance, we need to calculate the bar pattern speed. Following Ghosh et al. (2022) and Ghosh & Di Matteo (2024), we measure the bar pattern speed (Ω_{bar}) by fitting a straight line to the temporal variation of the phase angle (ϕ_2) of the $m = 2$ Fourier mode. The underlying assumption is that the bar rotates rigidly with a single pattern speed in that time interval. We follow this technique to compute the bar pattern speed (Ω_{bar}) as a function of time, for all thin + thick models considered here. The corresponding temporal evolution of bar pattern speed for three such thin + thick models is shown in Fig. 9. The bar pattern speed decreases drastically during the entire evolutionary phase of the bar (see Fig. 9). The radial locations where the bar pattern speed Ω_{bar} intersects with Ω, $\Omega - \kappa/2$, and $\Omega - \kappa/4$ determines the locations of
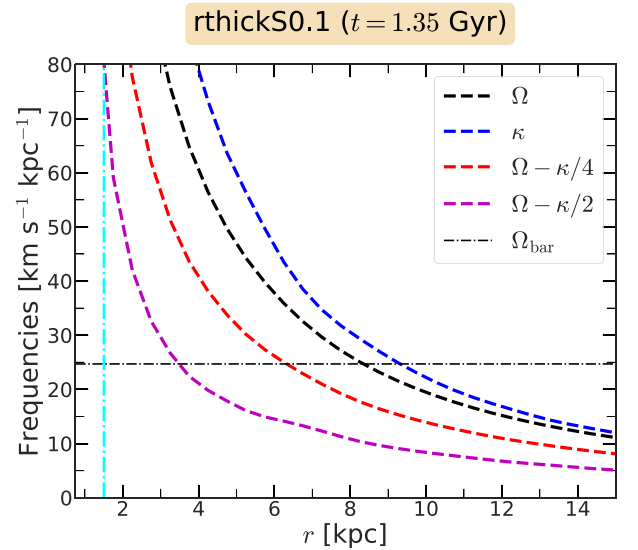

Figure 8. Radial variation of the circular frequency (Ω), epicyclic frequency (κ), $\Omega - \kappa/2$, and $\Omega - \kappa/4$ (see the legend), calculated at $t = 1.35\,\mathrm{Gyr}$ for the model rthickS0.1. The horizontal dash–dotted black line denotes the bar pattern speed (Ω_{bar}) at that epoch, while the vertical cyan line denotes the location of the dark gap (R_{DG}) at the same epoch.

the corotation, 2:1 inner Lindblad resonance, and 4:1 ultraharmonic resonance, respectively (see Fig. 8). We checked that the ratio of R_{CR} (location of bar corotation) to bar length (R_{bar}) always remains greater than 1.4, and this trend remains true for almost all thin + thick models considered here. Therefore, bars present in our thin + thick models qualify as *slow bars*. The detailed study of the temporal evolution of Ω_{bar} with varying thick disc mass fraction (f_{thick}) is
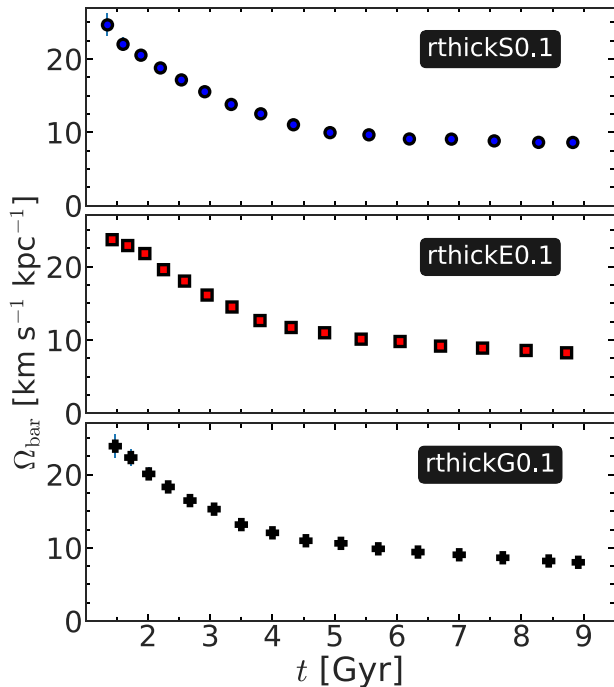
Figure 9. Temporal evolution of the bar pattern speed (Ω_{bar}) for three thin + thick models. In each case, the bar pattern speed decreases substantially over time.

beyond the scope of this work and will be addressed in a future study.

Using the rotation curve and the bar pattern speed, we calculated the locations of the corotation (R_{CR}), the 2:1 inner Lindblad resonance (R_{ILR}), and the 4:1 ultraharmonic resonance (R_{UHR}) at different times, for all thin + thick models considered here (e.g. see Fig. 8). We checked that the values of R_{CR}/R_{DG} remain well above unity for all thin + thick models considered here, thereby implying that the locations of the dark gaps are not associated with the corotation resonance of the bar in our bar models. This finding is similar to the conclusion drawn by Krishnarao et al. (2022). Furthermore, in Fig. 10, we show the temporal evolution of the quantities R_{DG}/R_{ILR} and R_{DG}/R_{UHR} as a function of bar age ($t_{bar\,age}$), for all thin + thick models considered here. The ratio of the R_{UHR} and the extent of dark gaps, R_{DG}, remains almost constant (especially at later bar evolutionary phases) and this holds true for almost all thin + thick models considered here. However, the ratio R_{DG}/R_{UHR} remains well below unity, for all the models, thereby demonstrating that the dark gaps are also *not* associated with the location of 4:1 ultraharmonic resonances for any of the models considered here, in contrast with the results presented in Krishnarao et al. (2022) and Aguerri et al. (2023). In addition, the temporal evolution of the ratio R_{DG}/R_{ILR} shows somewhat oscillatory behaviour in the initial bar growth phase; however, it saturates to a constant value towards the later bar evolutionary phase.

The most striking finding of this work is that in none of our barred models the extent of the dark gaps is associated with the bar resonances (corotation, inner Lindblad resonance, and 4:1 ultraharmonic resonance), as opposed to earlier studies in the literature (Krishnarao et al. 2022; Aguerri et al. 2023). We checked that the bar pattern speed values for our models are well below (approximately by a factor of 2) compared with those reported in Krishnarao et al. (2022) and Aguerri et al. (2023). We mention that the underlying mass model

(through the rotation curve) and the bar pattern speed together set the locations of different resonances associated with the bar. Therefore, the findings presented here clearly imply that the locations of the dark gaps are not *universally* associated with any of the resonances (of the bar) and depend on both the underlying mass model and the measured bar pattern speed. Furthermore, the bars in all our thin + thick models are slow rotators, i.e. $\mathcal{R}(= R_{CR}/R_{bar}) > 1.4$. We checked that most (about 90 per cent) of the MaNGA barred samples used in Aguerri et al. (2023) are fast rotators, i.e. $\mathcal{R}(= R_{CR}/R_{bar}) < 1.4$, and only about 10 per cent qualify as slow rotators ($\mathcal{R} > 1.4$). Similarly, in Krishnarao et al. (2022), most of the barred galaxies (for which the values of R_{CR} and R_{UHR} were reasonably measured) tend to qualify as fast rotators (within the large uncertainties with the corotation radius estimates; see discussions in section 4.1 of Krishnarao et al. 2022). Therefore, the question remains as to whether the association of the dark gap with bar resonances depends on different regimes of bars (i.e. slow versus fast). While our systematic study, as presented here, deals with slow bars, however, such a systematic study, dealing with fast bars, is largely missing in the literature and will be worth pursuing.

6 SUMMARY AND FUTURE PROSPECTS

In summary, we investigated the formation and the subsequent temporal evolution of the bar-induced dark gaps (along the bar minor axis) and their dynamical connection with the bar. We further examined the correlation between the properties of the dark gaps and the bar. We made use of a suite of N-body models of thin + thick discs (with varying thick disc mass fractions and different thin-to-thick disc scale length ratios), thereby allowing us to examine the formation and evolutionary trajectory of the dark gaps under diverse dynamical scenarios. Our main findings are listed below.

(i) A prominent bar always drives the generation of a dark gap along the bar minor axis. The strength of the dark gap, $\Delta\mu_{max}$, is strongly correlated with the strength of the bar, and this holds for all thin + thick models with varied geometric configurations. Similarly, the length of dark gaps is seen to remain strongly correlated with the bar length, provided a uniform definition is applied in both cases.

(ii) The formation and subsequent growth of dark gaps lead to substantial mass redistribution along the bar minor axis. For stronger dark gaps (and hence, for stronger bars), the mass-loss along the bar minor axis can reach up to ~60–80 per cent of the initial mass contained within the bar extent.

(iii) In all our thin + thick models, the ratio of R_{CR} and bar length R_{bar} remains above 1.4, thereby qualifying them as slow rotators ($\mathcal{R} > 1.4$). Furthermore, we did not find any robust and *universal* association of the location of dark gaps with the 4:1 ultraharmonic resonance or the 2:1 inner Lindblad resonances in any of our thin + thick models, in contrast with earlier studies.

To conclude, our systematic study demonstrates that the properties (strength and extent) of the dark gaps can be used as a robust proxy for the bar properties (strength and length). We mention that the thin + thick models used here do not contain any interstellar gas. The presence of a (dynamically) cold component, such as interstellar gas, makes the disc more susceptible to gravitational instabilities (e.g. see Jog & Solomon 1984; Jog 1996; Bertin 2000). Therefore, it would be worth investigating the secular evolution of bar-induced dark gaps in the presence of the interstellar gas.
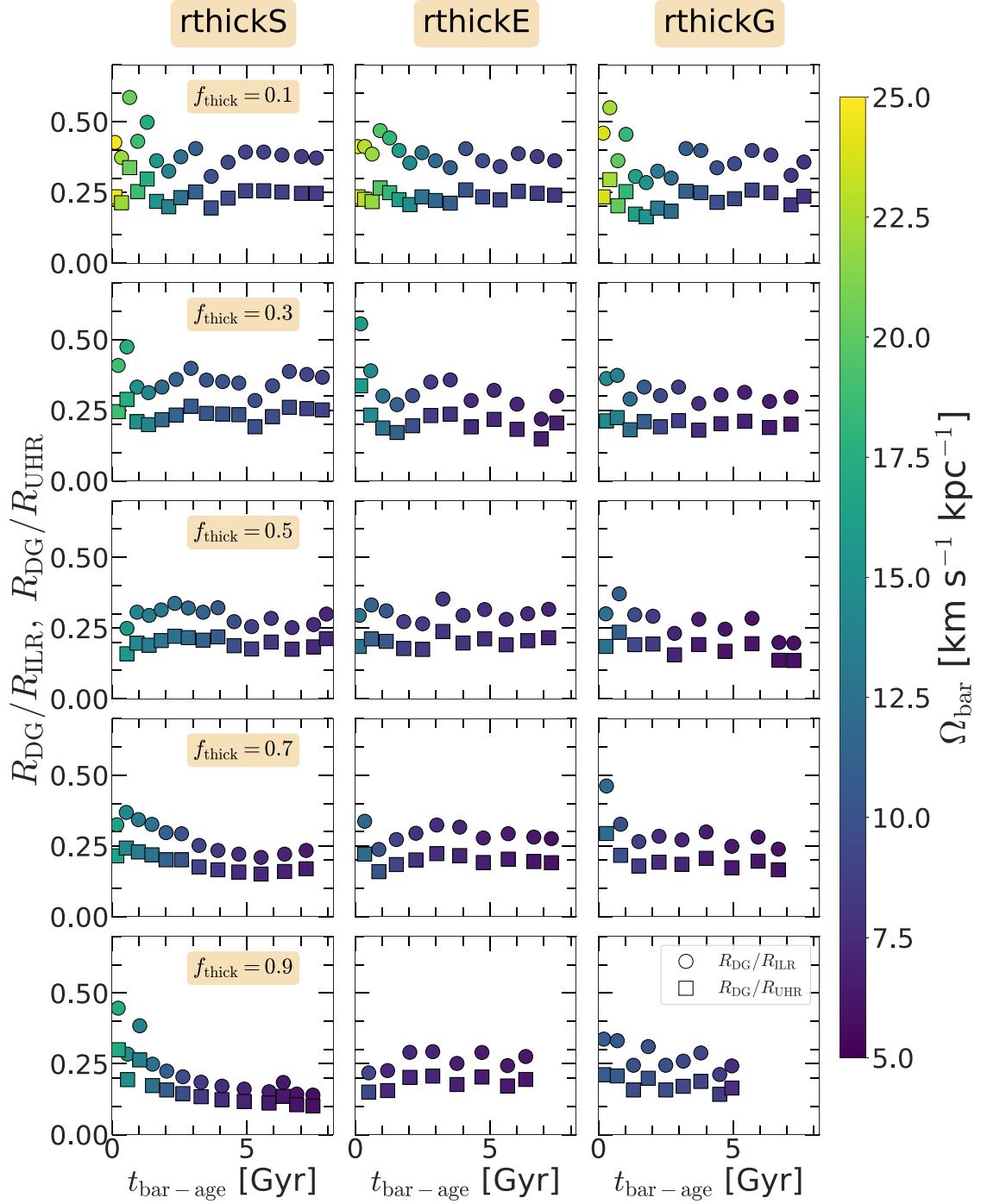
Figure 10. Evolution of the ratios R_{DG}/R_{ILR} (filled circles) and R_{DG}/R_{UHR} (filled squares) with bar age ($t_{bar\,age}$) for all thin + thick models considered here. The points are colour coded by the bar pattern speed (Ω_{bar}) values. Left panels show for the rthickS models, whereas middle panels and right panels show for the rthickE and rthickG models, respectively. The thick disc fraction (f_{thick}) varies from 0.1 to 0.9 (top to bottom), as indicated in the leftmost panel of each row.

DATA AVAILABILITY

The simulation data underlying this article will be shared on request to PDM (paola.dimatteo@obspm.fr).

REFERENCES

Aguerri J. A. L., Elias-Rosa N., Corsini E. M., Muñoz-Tuñón C., 2005, A&A, 434, 109

Aguerri J. A. L., Méndez-Abreu J., Corsini E. M., 2009, A&A, 495, 491

Aguerri J. A. L., D'Onghia E., Cuomo V., Morelli L., 2023, A&A, 670, A123

Athanassoula E., 2003, MNRAS, 341, 1179

Barnes J., Hut P., 1986, Nature, 324, 446

Barway S., Wadadekar Y., Kembhavi A. K., 2011, MNRAS, 410, L18

Bertin G., 2000, Dynamics of Galaxies. Cambridge Univ. Press, Cambridge

Binney J., Tremaine S., 2008, Galactic Dynamics, 2nd edn. Princeton Univ. Press, Princeton, NJ

Buta R. J., 2017, MNRAS, 470, 3819

Buta R., Laurikainen E., Salo H., Knapen J. H., 2010, ApJ, 721, 259

Buta R. J. et al., 2015, ApJS, 217, 32

Combes F., Sanders R. H., 1981, A&A, 96, 164

Comerón S. et al., 2011, ApJ, 741, 28

Comerón S., Salo H., Peletier R. F., Mentz J., 2016, A&A, 593, L6

Comerón S., Salo H., Knapen J. H., Peletier R. F., 2019, A&A, 623, A89

Contopoulos G., Grosbol P., 1989, A&AR, 1, 261

Costantin L. et al., 2023, Nature, 623, 499

Debattista V. P., Sellwood J. A., 2000, ApJ, 543, 704

Elmegreen B. G., Elmegreen D. M., Hirst A. C., 2004, ApJ, 612, 191

Erwin P., 2018, MNRAS, 474, 5372

Eskridge P. B. et al., 2000, AJ, 119, 536

Fragkoudi F., Di Matteo P., Haywood M., Gómez A., Combes F., Katz D., Semelin B., 2017, A&A, 606, A47

Fragkoudi F. et al., 2020, MNRAS, 494, 5936

Fragkoudi F., Grand R. J. J., Pakmor R., Springel V., White S. D. M., Marinacci F., Gomez F. A., Navarro J. F., 2021, A&A, 650, L16

Fragkoudi F., Grand R., Pakmor R., Gómez F., Marinacci F., Springel V., 2024, preprint (arXiv:2406.09453)

Gadotti D. A., 2011, MNRAS, 415, 3308

Gadotti D. A., de Souza R. E., 2003, ApJ, 583, L75

Ghosh S., Di Matteo P., 2024, A&A, 683, A100

Ghosh S., Saha K., Jog C. J., Combes F., Di Matteo P., 2022, MNRAS, 511, 5878

Ghosh S., Fragkoudi F., Di Matteo P., Saha K., 2023, A&A, 674, A128

Ghosh S., Fragkoudi F., Di Matteo P., Saha K., 2024, A&A, 683, A196

Guo Y. et al., 2023, ApJ, 945, L10

Jog C. J., 1996, MNRAS, 278, 209

Jog C. J., Solomon P. M., 1984, ApJ, 276, 114

Jogee S. et al., 2004, ApJ, 615, L105

Kasparova A. V., Katkov I. Y., Chilingarian I. V., Silchenko O. K., Moiseev A. V., Borisov S. B., 2016, MNRAS, 460, L89

Kim T., Gadotti D. A., Athanassoula E., Bosma A., Sheth K., Lee M. G., 2016, MNRAS, 462, 3430

Kormendy J., 1979, ApJ, 227, 714

Kraljic K., Bournaud F., Martig M., 2012, ApJ, 757, 60

Krishnarao D. et al., 2022, ApJ, 929, 112

Kruk S. J. et al., 2017, MNRAS, 469, 3363

Le Conte Z. A. et al., 2024, MNRAS, 530, 1984

Marinova I., Jogee S., 2007, ApJ, 659, 1176

Martig M. et al., 2021, MNRAS, 508, 2458

Masters K. L. et al., 2011, MNRAS, 411, 2026

Melvin T. et al., 2014, MNRAS, 438, 2882

Menéndez-Delmestre K., Sheth K., Schinnerer E., Jarrett T. H., Scoville N. Z., 2007, ApJ, 657, 790

Miyamoto M., Nagai R., 1975, PASJ, 27, 533

Nair P. B., Abraham R. G., 2010, ApJ, 714, L260

Pinna F. et al., 2019a, A&A, 623, A19

Pinna F. et al., 2019b, A&A, 625, A95

Planck Collaboration VI, 2020, A&A, 641, A6

Plummer H. C., 1911, MNRAS, 71, 460

Pohlen M., Balcells M., Lütticke R., Dettmar R. J., 2004, A&A, 422, 465

Rodionov S. A., Athanassoula E., Sotnikova N. Y., 2009, MNRAS, 392, 904

Rosas-Guevara Y. et al., 2022, MNRAS, 512, 5339

Scott N., van de Sande J., Sharma S., Bland-Hawthorn J., Freeman K., Gerhard O., Hayden M. R., McDermid R., 2021, ApJ, 913, L11

Sellwood J. A., Wilkinson A., 1993, Rep. Prog. Phys., 56, 173

Semelin B., Combes F., 2002, A&A, 388, 826

Sheth K. et al., 2008, ApJ, 675, 1141

Simmons B. D. et al., 2014, MNRAS, 445, 3466

Smail I. et al., 2023, ApJ, 958, 36

Tsukui T., 2023, Bar-driven galaxy evolution at z=4.4? Zenodo. Available at: https://doi.org/10.5281/zenodo.8245961

Yoachim P., Dalcanton J. J., 2006, AJ, 131, 226

APPENDIX A: CORRELATION BETWEEN PROPERTIES OF BARS AND DARK GAPS

Fig. A1 shows the face-on surface brightness distribution of all 15 thin + thick models, calculated at the end of the simulation run ($t = 9$ Gyr). Even a mere visual inspection of Fig. A1 reveals the presence of conspicuous dark gaps, along the bar minor axis, for almost all thin + thick models considered here.

In Fig. A2, we show the radial profiles of $\Delta\mu$ as a function of time for three thin + thick models, namely rthickS0.1, rthickS0.7, and rthickS0.9. As seen clearly, the temporal evolution of radial profiles of $\Delta\mu$ shows variation across the three thin + thick models considered here. While for the model rthickS0.1, the peak location of $\Delta\mu$ progressively shifts towards the outer disc region with time, however, for the model rthickS0.9, the peak location of $\Delta\mu$ does not shift appreciably towards the outer disc region with time.
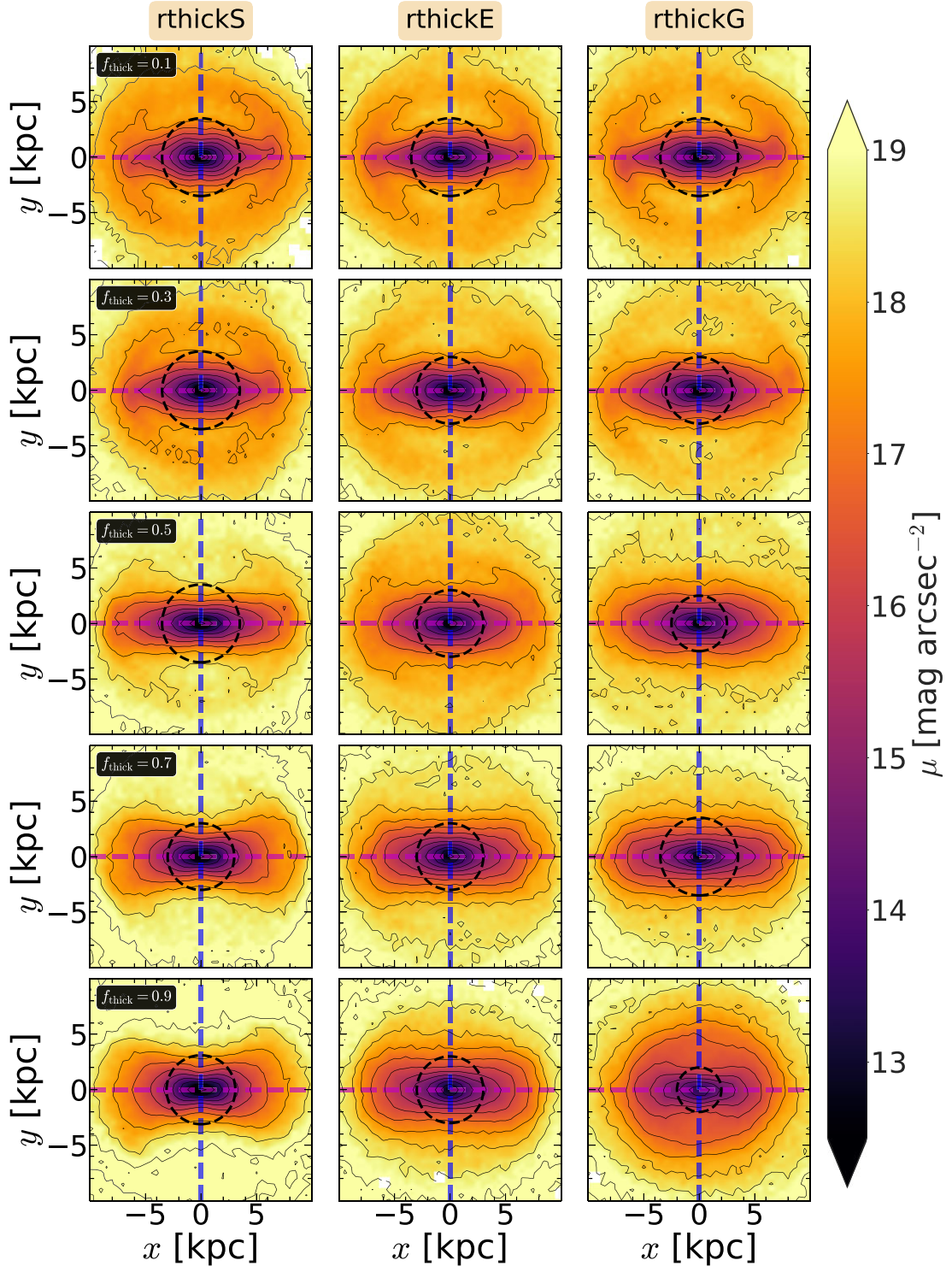
Figure A1. Face-on surface brightness distribution, calculated at the end of the simulation run ($t = 9\,\mathrm{Gyr}$), for all thin + thick models considered here. Black solid lines denote the contours of constant surface brightness. For each case, the bar is placed along the x-axis. The magenta and the blue dashed lines denote the bar major and minor axis, respectively. The black dashed circle denotes the location of maximum brightness contrast ($\Delta\mu_{\mathrm{max}}$); for details see the text. Left panels show the surface brightness distribution for the rthickS models, whereas middle panels and right panels show the surface brightness distribution for the rthickE and rthickG models, respectively. The thick disc fraction (f_{thick}) varies from 0.1 to 0.9 (top to bottom), as indicated in the leftmost panel of each row. A magnitude zero-point (m_0) of 22.5 mag arcsec^{-2} and $\Upsilon_{\mathrm{T}}/\Upsilon_{\mathrm{t}} = 1.2$ are used to create the surface brightness from the intrinsic particle distribution. Here, 1 arcsec = 1 kpc.
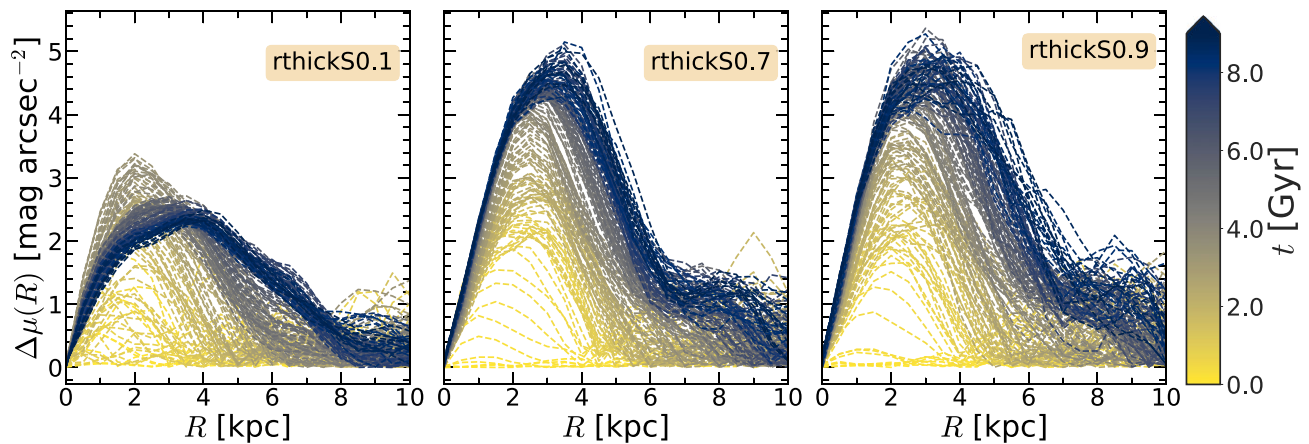
Figure A2. Radial variation of $\Delta\mu$ as a function of time (see the colour bar) for three thin + thick models, namely rthickS0.1, rthickS0.7, and rthickS0.9. A magnitude zero-point (m_0) of 22.5 mag arcsec^{-2} and $\Upsilon_T/\Upsilon_t = 1.2$ are used to create the surface brightness from the intrinsic particle distribution. Here, 1 arcsec $= 1$ kpc.

This paper has been typeset from a T$_E$X/L^{A}T$_E$X file prepared by the author.